The Lipid-Associated 3D Structure of SPA, a Broad-Spectrum Neuropeptide Antagonist with Anticancer Properties

David A. Keire,*† Mohanraja Kumar,*† Weidong Hu,‡ James Sinnett-Smith,*† and Enrique Rozengurt*†
*CURE: Digestive Diseases Research Center, VA Greater Los Angeles Healthcare System, Los Angeles, California:
†Digestive Diseases Division, University of California Los Angeles School of Medicine, Los Angeles, California; and
‡Division of Immunology, Beckman Research Institute of the City of Hope, Duarte, California

ABSTRACT [D-Arg^1, D-Trp^{5,7,9}, Leu^{11}] substance P (SPA) belongs to a family of peptides including antagonist G and SpD that act as broad-spectrum neuropeptide antagonists at several peripheral receptors. The lipid-induced structure of these peptides may be important for the receptor interactions of these analogs. Thus we describe the tertiary structure of SPA in the presence of sodium dodecylsulfate micelles at pH 5.0, and 25°C as determined from two-dimensional ^{1}H-NMR data recorded at 500 MHz. The resulting three-dimensional structure can be generally described as two type IV nonstandard turns around Arg^1*, Pro^2, Lys^3, and Pro^4 and Gln^6, Trp^7*, Phe^8, and Trp^9* residues, respectively, inserted into the interfacial region of the micelles (the asterisks denote D-form amino acid). These turns juxtapose the N- and C-termini of SPA and may form the basis of this peptide's unique ability to inhibit peptide receptor interactions at multiple receptor types.

INTRODUCTION

Neuropeptides act as signals to regulate numerous physiological functions centrally and peripherally via interactions with G-protein coupled receptors (1). These molecular messengers are also potent growth factors for normal and cancerous cells (2). For example, small cell lung cancer (SCLC) and pancreatic cancer cells stimulate their own proliferation via autocrine and paracrine actions of multiple peptide hormones including; gastrin-releasing peptide, gastrin, cholecystokinin, neurotensin, galanin, vasopressin, and bradykinin (2,3). For this reason, therapeutic agents targeting one receptor type cannot effectively suppress SCLC cell growth.

Broad-spectrum neuropeptide antagonists (BNSAs) are a class of therapeutic compounds that address this multi-peptide proliferative response by acting as antagonists at multiple peptide-hormone receptors. For example, substance P analogs (e.g., [Arg^6, D-Trp^{7,9}, N^{me}Phe^8] substance P(6-11) (antagonist G), [D-Arg^1, D-Phe^5, D-Trp^{7,9}, Leu^{11}] substance P (SpD), and [D-Arg^1, D-Trp^{5,7,9}, Leu^{11}] substance P (SPA)) have been shown to inhibit the growth of SCLC cells in vivo and in vitro (4,5). In initial studies, these broad-spectrum neuropeptide antagonists were shown to be competitive inhibitors of the mitogenic neuropeptides at low micromolar concentrations (4,6,7). Finally, a recent monograph has shown that SPA attenuates tumor growth in pancreatic cancer via antiproliferative and antiangiogenic mechanisms (8).

The molecular mechanisms for the inhibition of multiple neuropeptide ligand/receptor interactions by substance P analogs are unknown. Because these analogs act at multiple receptors, one supposition is that these receptors share a similar binding pocket for substance P analogs that overlaps with the binding site for the native neuropeptide ligands. Thus, the spatial arrangement of the substance P analog side chain and backbone moieties that changes the pharmacology of the neuropeptide receptors would be useful in the design of future more high affinity versions of the peptide.

Structural studies of several substance P analogs and members of the substance P family of peptides have been performed in aqueous and hydrophobic solutions by a variety of methods. For example, [D-Arg^1, D-Trp^{7,9}]-SP, [D-Arg^1, D-Pro^2, D-Trp^{7,9}, Leu^{11}]-SP, and [D-Pro^2, D-Trp^{7,9}]-SP have been examined in aqueous solution and in the presence of DMSO or hexafluoroacetone (HFA) by circular dichroism (CD) and NMR (9). Prabhu et al. concluded that these SP analogs showed a ''high'' preference for β-turns in DMSO and H_2O while in HFA the C-terminal residues adopted a helical conformation. The open question is whether or not the solution conformation of an eleven amino acid peptide can be stable enough in solution to measure a meaningful tertiary structure. Furthermore is this solution state tertiary structure the biologically active form of the peptide?

Ideally, one would obtain the structure of a peptide ligand bound to its receptor. Unfortunately, for most G-protein coupled receptors of pharmaceutical interest it is not possible to measure the tertiary structure of the membrane bound receptor or of the ligand/receptor complex. To our knowledge, only one study has the reported structure of a peptide agonist bound to a G-protein coupled receptor (10): Inooka et al. determined the structure of a pituitary-adenylate-cyclase-activating polypetide analog (PACAP(1-21)-NH_2) bound to the PACAP receptor. Their study required the expression of milligram quantities of receptor, solubilization of the receptor in digitonin, development of a ligand with lowered affinity for the receptor, and collection of NMR data on an 800-MHz spectrometer (10). Therefore, because of the

Submitted May 18, 2006, and accepted for publication September 6, 2006.

Address reprint requests to David A. Keire, VA GLAHS, Bldg. 115, Rm. 111B, 11301 Wilshire Blvd., Los Angeles, CA 90073. Tel.: 310-478-3711, Ext. 41828; Fax: 310-268-4963; E-mail: dkeire@ucla.edu.

0006-3495/06/12/4478/12 $2.00

doi: 10.1529/biophysj.106.089292

difficulty in obtaining ligand/receptor three-dimensional (3D) structure, the structure of the ligand in solution in the absence of receptor has been used for structure based-drug design.

A less difficult approach is to solve the tertiary structure of the peptide ligand in the presence of lipid mimetics (11,12). Previously, it has been proposed that the membrane surface conformation and orientation of a peptide at a lipid bilayer may be more important to the peptides affinity and specificity for a given receptor than its solution structure (13). In this model a peptide may associate with the cell surface lipids by insertion of hydrophobic residues, and electrostatic interactions with charged lipid headgroups to form a unique 3D conformation.

This lipid-induced conformation is transported via the bilayer to its receptor-binding pocket located in a transmembrane portion of the receptor. If this model is correct the lipid-induced tertiary structure of the peptide would be the conformation that binds the receptor. This approach is lent credence by the work on PACAP because these authors observed that the lipid micelle bound structure and the receptor bound structure of their PACAP analog shared a common helical region (10). Therefore, in this work, we report the 3D structure of the substance P analog, SPA, in the presence of lipid micelles. Micelles made up of perdeuterated monomers have the property of adding little proton background to the spectra and enabling effective isotropic reorientation for bound peptides. Other NMR methods show promise for elucidating peptide structures in the presence of lipid vesicles, oriented lipid bilayers, or lipid bicelles (e.g., (14) and references therein).

Previously our laboratory has solved the micelles associated tertiary structure of SP (Arg-Pro-Lys-Pro-Gln-Gln-Phe-Phe-Gly-Leu-Met-amide) in the presence of DPC and SDS micelles and examined in detail the amide-exchange and longitudinal (T_1) and transverse (T_2) relaxation time changes upon micelle association (15,16). From these data a well-characterized model of the orientation, dynamics, and tertiary structure of substance P was developed (16). In this model the N-terminal Arg-Pro-Lys-Pro- residues are located above the micelle surface in a number of conformations, at residue Gln^5 or Gln^6 the peptide is inserted in a nonstandard turn containing the residues Phe-Phe-Gly and protected from solvent exchange (the C-terminal residues are Leu^{10} and Leu^{11} are more exposed to amide exchange) (16). We postulated that the structure of the Gln-Phe-Phe-Gly-Leu portion of the peptide was an important recognition element for binding to the NK-1 receptor. Similarly Auge' et al. (14) using a transfer NOE experiments in the presence of perdeuterated DMPC (1,2-dimysteroyl-*sn*-glycero-3-phosphocholine-d_{72}) vesicles reported a substance P structure that consisted of nonstandard turns in the C-terminus of the molecule. In addition molecular dynamic calculations with substance P in the presence of explicit SDS micelles in water showed that substance P preferentially selects the lipid-water interface and adopts a nonstandard turn structure for residues Gln-Gln-Phe-Phe (17).

Few studies of the tertiary structures of substance P analogs that act as antagonists at NK-type receptors have been reported. Whitehead et al. reported that the [D-Pro^2, D-Phe^7, D-Trp^9]-SP and [D-Arg^1, D-Pro^2, D-Trp^7, D-His^9]-SP had tertiary structures in the presence of SDS micelles that consisted of a poorly defined helical mid-region with a β-turn in the C-terminal section of the peptide (18). These authors suggest that the differences between the partial helical nature of NK-A, NK-B, and substance P (NK-receptor agonist peptides) and β-turn structures of the NK-receptor antagonists determine their biological activity.

The insertion of D-amino acids is known to disrupt helical structures in solution and in the presence of lipid membranes (e.g., (19,20)). Thus the presence of nonstandard turns in D-amino acid substituted broad-spectrum-neuropeptide antagonists are to be expected. In this work we present the structure of another D-amino acid substituted substance P analog (SPA) in the presence of SDS micelles for comparison with those determined by Whitehead et al. (18).

MATERIALS AND METHODS

The SPA peptide was obtained from the UCLA Peptide Synthesis facility. The peptides were purified by reverse phase HPLC. Analytical HPLC showed their purity was above 90% and the correct sequence was verified by mass spectrometry. The pH of the H_2O solutions was adjusted to pH 5.0 by the addition of HCl and NaOH; measurements were performed using an Orion Model 601 pH meter fitted with a combination electrode for 5 mm NMR tubes (Ingold Electrodes, Wilmington, MA). The perdueterated d_{25}-SDS was purchased from C/D/N Isotopes (Pointe-Claire, Quebec, Canada) and used in all the NMR experiments. Standard aqueous buffers were used for electrode calibration at pH 4 and 7.

Circular dichroism and fluorescence studies

CD studies were performed on a Jasco J-710 spectropolarimeter at 20°C. A sample of 80 μM SPA, 50 mM SDS, and a pH of 5.0 was freshly prepared and the spectra acquired. Ten scans were averaged from 185 to 260 nm at a rate of 100 nm/min. A 1-mm path length cell was used and the intensities are expressed as molar ellipticity $[\theta]_{222}$ (deg cm^2dmol^{-1}). The CD instrument was calibrated using D-10 camphorsulphonic acid. The peptide concentration of the sample was prepared by dissolving weighed quantities of peptide powder in SDS micelle solutions.

Fluorescence emission spectra were recorded on Photon Technology Instrumental spectrofluorimeter (Monmouth Junction, NJ). The concentration of both NATA (N-acetyl tryptophan amide) and SPA were 40 μm dissolved in 50 mM SDS in water at a pH of 5.0. Three scans were of the emission spectra were recorded and averaged between 300 and 400 nm, at 1-nm increments using 1 mm quartz cell with a scan speed of 100 nm/min at room temperature for both NATA and SPA. The excitation wavelength was fixed at 280 nm with both excitation and the emission slit width set to 1 nm.

NMR studies

NMR experiments were performed on a Bruker 500 MHz spectrometer in the City of Hope NMR facility with a 5 mm triple resonance xyz-gradient probe and the air temperature regulated at 25°C. Solutions for NMR analysis

of SPA were made at ~1 mM peptide concentration in 750 μl of 90% H_2O/10% D_2O in water alone or 50 mM perdueterated SDS-micelle at pH 5.0. Chemical shift assignments for SPA in solution were obtained by the standard method using total correlation spectroscopy (TOCSY) (21), and nuclear Overhauser effect spectroscopy (NOESY) (22) pulse sequences. All chemical shifts were reference to external 2,2-dimethyl-2-silapentane-5-sulfonic (DSS) acid in D_2O.

Phase-sensitive NOESY data were collected for conformational analysis of the SPA solutions with the Bruker library pulse program (23). A total of 8K points were collected in t_2 (64 transients per increment), a 100-ms or 200-ms mixing time was used, and 480 complex points acquired in t_1 using States-TPPI (24,25). A relaxation delay of 1.5 s was used between transients. The transmitter channel was used for excitation and observation of the 6000 Hz proton frequency range. Water suppression was attained with a Watergate sequence using flip-back pulses with radiation damping suppression using gradients in t_1 (26). Data was processed with zero filling to 8K points in F2, 2K points in F1, and sinebell squared or Gaussian apodization functions in both F1 and F2.

Phase-sensitive TOCSY spectra were collected to aid in the assignment of SPA chemical shifts with the Bruker library pulse program (27). This pulse sequence performs homonuclear Hartmann-Hahn transfer using a DIPSI-2 sequence for mixing. Water suppression is performed using excitation sculpting with gradients. A total of 8K points were collected in t_2 (32 transients per increment), a 50-ms mixing time was used, and 480 points were collected in t_1 using States-TPPI. Data was processed with zero filling to 8K points in F2, 2K points in F1, and sinebell squared or Gaussian apodization functions in both F1 and F2.

NMR structure calculations

Structures for SPA were determined using XPLOR software, Version 3.1 (28). For SPA 100- and 200-ms NOESY experiments provided the 83 distance restraints needed for XPLOR 3D structure calculations. Distance restraints were input as 1.8–6.0 Å distance ranges and standard pseudo-atom corrections were used where appropriate (29). The constraint set for SPA contained 25 intraresidue, 37 (i, i + 1), 8 (i, i + 2), 2 (i, i + 3), 6 (i, i + 4), and 5 (3i, i15) NOEs between protons on various residues. The greater than or equal to i, i + 5 NOEs can only be present in a stable folded conformation of SPA.

These constraints were used for the calculation of SPA structures satisfying the distance boundaries. One hundred and fifty one embedded-distance-geometry structures were obtained using the ''sa'' protocol with a force constant of 50 kcal on the NOE-derived distance restraints. The LTOD patch was used in the generate step of X-PLOR to get a coordinate file with D-form Arg and Trp residues. The topallhdg.pro was modified to have the D-form impropers. The parameter file ''parallhdg.pro'' was employed in this procedure. Once structures were generated in this fashion, they were subjected to an additional 10 ps of simulated annealing by the ''refine'' protocol (28). Out of the resulting 45 structures with no distance violations >0.3 Å, 20 were chosen that had the lowest NOE energies. XPLOR generated structures were visualized with the program Insight (Version 2000, Accelrys, San Diego, CA).

RESULTS

CD data

CD spectra from 190 to 260 nm are shown in Fig. 1 for SPA in solution and for SPA in SDS micelles at pH 5.0 (the pH where the NMR data was collected). The spectrum for SPA in solution has two negative minima at 200 and 213 nm, a positive maximum at around 229 nm. These spectral features for SPA in aqueous solution at pH 5.0 could describe a mixture of random coil ([−]195–197 nm), β-turn (e.g., [+]190 and [−]213) conformers, and the contribution of the tryptophan indole ring orientation with respect to the peptide backbone ([+]229 nm) (30).

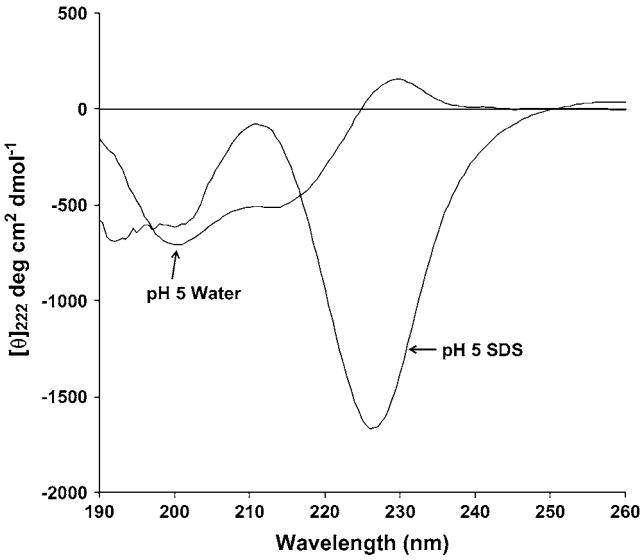

FIGURE 1 Molecular ellipticity versus wavelength plots are shown for solutions of 80 μM SPA. Spectra on samples in water alone or in the presence of 50 mM SDS micelles at pH 5 and 20°C are compared. The change in the pattern of the spectra indicates association of the peptide with the micelle with an alteration in the peptides conformation.

In the presence of SDS micelles a conformational shift in SPA occurs compared to the structure in water alone (Fig. 1). For SPA in the presence of micelles a broad minimum around 200 nm and a sharper minimum 226 nm are observed. The peak at 226 nanometers is characteristic of tryptophan residues of which there are three in SPA (Trp^{5*}, Trp^{7*}, and Trp^{9*}). Woody has observed that because of the low symmetry of the tryptophan side chain with respect to rotation about the χ2 bond (a dihedral formed by Cβ and Cγ carbons) the sign of the 229-nm band can change markedly with alterations in indole orientation (31). Upon association with the SDS micelles the SPA indole moieties assume an altered orientation with respect to the peptide backbone that causes a major change in the sign of the ellipticity. If SPA has a turn structure in the presence of micelles then these features could be masked by the presence of this strong 226 nm ellipticity (32). Not observed are bands that would indicate the presence of residues in a helical ([+]195, [−]208, and [−]222 nm), random coil ([−]195–197 nm), or beta-sheet ([+]195 and [−]215 to 217 nm) conformations. A similar pattern of ellipticity was observed for SPA in the presences of DPC micelles (data not shown).

Fluorescence data

We compared the fluorescence of SPA in water alone or in the presence of SDS micelles, with NATA (N-acetyl

tryptophan amide) to examine the effects of the different solution conditions on the environment of the three tryptophan residues in SPA. The fluorescence emission spectra were recorded between 300 and 400 nm, at an excitation wave length of 280 nm. The spectra were collected on samples with 40 μM peptide or 40 μM NATA concentrations in water or in solution with SDS micelles present at pH 5.0 and room temperature. In Fig. 2, SPA or NATA in water have emission maximum of 348 and 352 nm, respectively. In addition the SPA and NATA spectra in the presence of SDS micelles have a shoulder not present in the NATA in water only spectrum (at ~330–335 nms) suggesting this blue-shifted shoulder is associated with the presence of the micelles. In general when a peptide containing a fluorescent amino acid is inserted into a more hydrophobic environment by associated with a lipid surface the wavelength of maximal fluorescence of the bound or folded species is blue-shifted (e.g., from 350 nms to 325 nms) and an increase in intensity is observed (33). By contrast, in the case of SPA association with SDS micelles, although there is a small blue shift from 350 to 346 nm, a large decrease (42%) in intensity of the signal relative to the value in water alone is observed. This pattern has been attributed to location of the tryptophan residues in the interfacial region of the lipid-water interface (34). Thus the negative charge of the lipid headgroup alters the fluorescence quantum yield of the tryptophan either by a direct quenching mechanism or indirectly by surface polarity effects (dielectric) (35). Therefore the association of SPA with SDS micelles results in the insertion of SPA tryptophan residues into interfacial region of the water-micelle surface. The intrinsic preferential localization of tryptophan containing peptides to the interfacial region of membrane surfaces has been proposed before by Jacobs and White (36) and tryptophan residues have been shown to found at the level of the carbonyl group in phophatidylcholine membranes (37).

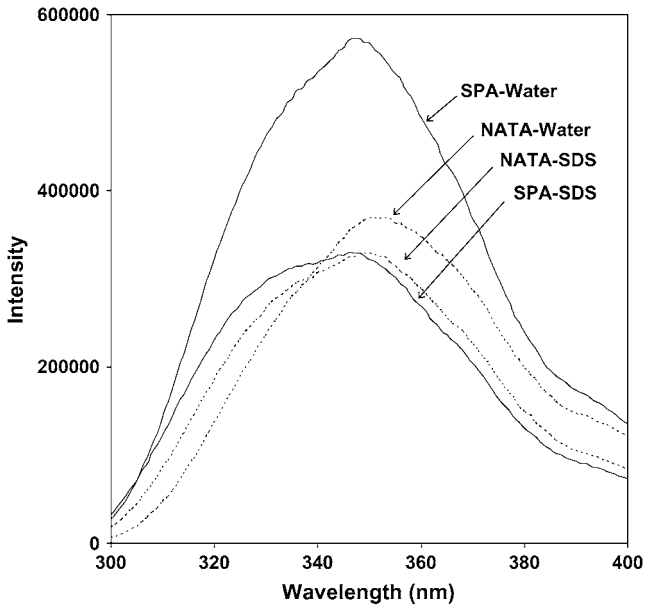

FIGURE 2 Fluorescence emission intensity versus wavelength plots are shown for solutions of 40 μM SPA (*solid line*) or 40 μM NATA (*dashed line*). A 280-nm excitation wavelength was used. Spectra in water alone or in the presence of 50 mM SDS for both compounds are compared. The observed decrease in fluorescence intensity in the presence of the lipid micelles is attributed to quenching caused by insertion of the tryptophan indole rings into the hydrophobic lipid environment.

NMR data

Essentially complete chemical shift assignments were obtained for SPA in aqueous solution alone and in the presence of SDS micelles (Table 1). In addition ROE and NOE intensity values were obtained for SPA in aqueous solution and in the presence of SDS micelles, respectively. Because no NOEs were observable for SPA in aqueous solution alone ($\omega\tau_c \sim 1$) the ROESY pulse sequence was used to probe for the presence of stable solution state tertiary structure in the absence of lipids.

For SPA in aqueous solution sequential NH to NH ROEs were observed in the 100-ms ROESY spectrum (not shown) between residues on Gln^6, Trp^7*, Phe^8, Trp^9*, Leu^{10}, and Leu^{11} (the asterisks denote D-form amino acids). In addition, sequential CαH to NH ROEs were observed for Gln^6 to Trp^7*, Trp^9* to Leu^{10}, and Leu^{10} to Leu^{11} (data not shown). Although several additional sequential backbone to side chain and side chain to side chain ROEs were found, no longer range ROEs were observed. These ROE interactions suggest that the C-terminal portion of SPA folds into a conformation that is stable for the millisecond timescale necessary to generate through-space magnetization transfer between protons in the rotating-frame. However, the lack of longer range ROEs suggests peptide conformational flexibility in solution.

The ^{1}H-NMR signals observed for SPA in aqueous solution broaden and shift upon association with the slower tumbling SDS micelles (Fig. 3). A single set of shifted proton signals is observed indicating a unique stable lipid-associated form of the peptide. Similar spectra were observed for the association of substance P with dodecylphosphocholine (DPC) and SDS micelles (15,16). The partition coefficient of SP into anionic micelles has been reported to be ~10^2–10^6 M^{-1} (14). Thus in the presence of an anionic micelle surface under the solution conditions used in our studies, SP is essentially completely bound. Because SPA is more hydrophobic than SP (containing three tryptophan residues), and SP-like chemical shift changes are observed in SPA upon titration with SDS we conclude that SPA is essentially completely bound to the SDS micelle surface under the conditions used in this work.

The chemical shifts of SPA CαH protons in solution or in the presence of SDS micelles minus the random-coil solution-state chemical shifts of Wishart are plotted in Fig. 4, *a* and *b*, respectively (38). In water alone (Fig. 4 *a*) significant differences from random-coil values ($>\pm0.2$

TABLE 1 ^{1}H-NMR assignments for SPA in solution and in the presence of SDS micelles

	NH	C$^{\alpha}$H	C$^{\beta}$H	C$^{\gamma}$H	C$^{\delta}$H	Others
(D)Arg^1*	n.a.	4.36	1.91	1.68	3.23	δNH = 7.25
(D)Arg^{1†}	n.a.	n.a.	1.53	1.30	2.91	δNH = 7.34
Pro^2*		n.a.	1.71/1.62	1.49/1.37	3.15/3.32	
Pro^{2†}		4.49	2.20/1.91	1.80	3.74/3.55	
Lys^3*	8.28	4.36	1.49/1.56	1.27	1.42	C$^{\varepsilon}$H = 2.86/εNH$_3$ = n.a.
Lys^{3†}	8.14	4.49	1.61/1.50	1.31	1.93/1.72	C$^{\varepsilon}$H = 3.20/εNH$_3$ = 7.15
Pro^4*		4.37	1.94/2.18	1.94	3.58/3.72	
Pro^{4†}		4.52	1.70/1.60	1.56/1.29	3.58/3.43	
(D)Trp^5*	7.15	4.52	3.21			2H-7.10 4H-7.52 5H-7.16 6H-7.22 7H-7.47 NH-10.09
(D)Trp^{5†}	7.25	4.51	3.07			2H-6.94 4H-7.40 5H-6.96 6H-7.01 7H-7.28 NH-9.44
Gln^6*	7.89	4.29	1.55/1.61	1.71		δNH2 = 6.95/7.43
Gln^{6†}	7.76	4.20	1.75	1.93		δNH2 = 6.74/7.27
(D)Trp^7*	8.38	4.44	3.03			2H-6.67 4H-7.56 5H-7.16 6H-7.22 7H-7.50 NH-10.20
(D)Trp^{7†}	7.86	4.58	3.05/2.94			2H-7.12 4H-7.40 5H-7.01 6H-7.08 7H-7.38 NH-9.85
Phe^8*	8.07	4.70	2.71/2.82			2,6H = 6.96 3,5H = 7.26 4H = n.a.
Phe^{8†}	7.76	4.56	2.98			2,6H = 7.20 3,5H = 7.10 4H = n.a.
(D)Trp^9*	7.92	4.14	2.47/2.97			2H-7.12 4H-7.52 5H-7.16 6H-7.25 7H-7.43 NH-10.09
(D)Trp^{9†}	8.24	4.31	3.17/3.06			2H-7.14 4H-7.49 5H-7.03 6H-7.12 7H-7.64 NH-10.06
Leu^{10}*	7.97	3.72	1.01/1.15	0.52	0.23/0.33	
Leu^{10†}	6.78	4.00	1.42	1.24	0.60/0.52	
Leu^{11}*	7.82	4.16	1.55/1.64	n.a.	0.77/0.86	NH$_2$ = 6.67/7.13
Leu^{11†}	7.83	4.21	1.69	1.54	0.83/0.75	NH$_2$ = 6.84/7.06

n.a. = not assigned; residues 1,5,7, and 9 are D-form amino acids.
*1 mM SPA in 90% H_2O/10% D_2O; pH = 5.0.
†SPA in SDS micelles (1:50) in 90% H_2O/10% D_2O; pH = 5.0.

ppm) are observed for residues Trp^9* and Leu^{10}. By contrast shifts of SPA CαH protons in the presence of micelles (Fig. 4 *b*) show a different pattern and a greater than 0.2 ppm difference from random-coil values for residue Trp^9*. For SPA in water alone, the chemical shifts of the β, γ, and δ side-chain protons of Leu^{10} are also significantly shifted from their random coil values by -0.64, -1.12, and -0.71 ppm, respectively. The unusual water only chemical shifts for the Leu^{10} side-chain protons are attributed to ring-current shifts caused by the proximity of the Trp^7*, Phe^8, and Trp^9* aromatic rings. In addition, $^3J_{NH\text{-}C\alpha H}$ scalar coupling constants for SPA residues in solution ranged from 6 to 8 Hz except for residues Trp^{7*}and Trp^{9*} that had values of 5.4 and 4.2 Hz, respectively. Consistent with the ROE data, these chemical shift differences and coupling constant data suggest a preference for a folded conformation in the Trp^7*, Phe^8, Trp^9*, Leu^{10} portion of SPA in water alone.

The chemical shifts of SPA NH and CαH protons in the presence of SDS micelles minus their solution-state chemical shifts are plotted in Fig. 4 *c*. Significant differences are observed for either the NH and/or CαH proton chemical shift values of residues Trp^5*, Gln^6, Trp^9*, and Leu^{10}. These chemical shift changes from the SPA solution-state values indicate that these SPA residues associate with the SDS micelle surface and concomitantly alter the environment of the observed protons via changes in structure and/or interaction with lipid moieties.

The NOESY and TOCSY spectra acquired on solutions of SPA in the presence of SDS micelles enabled structure calculations to determine the tertiary structure of SPA in a lipid environment (Fig. 5, *a–c*). A sequence of NH to NH connectivities is observed in the 100-ms and 200-ms NOESY spectra between residues Trp^5* to Gln^6 and Phe^8 through Leu^{11}. The NH to NH connectivity between residues Gln^6, Trp^7*, and Phe^8 are obscured due to overlapping chemical shift values. In addition, sequential NH to CαH NOEs were observed for Trp^5* to Gln^6 and Trp^9* to Leu^{11} (Fig. 6). The NH to CαH NOEs between Gln^6 and Trp^9* are masked by overlapping chemical shift values. Of note, there are signals at the sites of Gln^6 to Trp^9* NH to CαH NOEs but they cannot be unambiguously assigned. In contrast to SPA in water alone, a number of long range NOEs were observed for SPA in the presence of SDS micelles. For example, NOEs are observed between Leu^{11} side-chain protons and Trp^5*, Trp^7*, and Arg^1* side-chain protons (Figs. 5 and 6). A list of the observed *i*, *i* + 2 and greater NOEs used in the structure calculations is presented in Table 2.

X-PLOR structure calculations were based on a set of 83 NOEs derived from the 100-ms and 200-ms NOESY spectra acquired on an aqueous solution of 1 mM SPA in 90% H_2O/

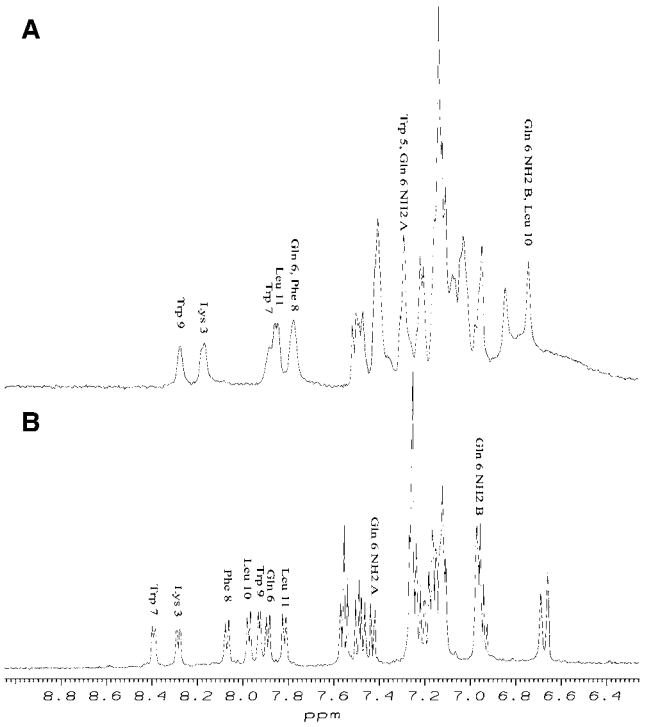

FIGURE 3 A plot of the 6.5–8.9 ppm frequency range of the 500 MHz 1D ^{1}H-NMR spectra of 1 mM SPA in the presence of 50 mM SDS micelles (*a*) or in water alone (*b*). Selected amide proton signals are labeled with their assigned residues. The broadened and shifted amide proton signals are characteristic of association of the peptide with the larger molecular weight slower tumbling micelles.

10% D_2O at pH 5.0 with 50 mM SDS monomer present. The distance constraint set was provided as input to the X-PLOR program. One hundred and fifty-one initial structures were generated by the simulated annealing protocol and further refined by molecular dynamics and energy minimization (see Materials and Methods). An overlay was produced of the 20 best structures that had the lowest NOE energies from a set of 45 structures that had no NOE violations >0.3 Å. Fig. 7 *a* depicts a stereo-view of the backbone (NH, CαH, CO) overlay and Fig. 7 *b* shows the stereo-view of the heavy atom overlay of six structures (NH, CαH, CO, and side-chain carbon, oxygen, and nitrogen). The calculated structure root-mean-square deviations (RMSDs) are 0.78 ± 0.24 for the backbone atoms and 1.30 ± 0.33 Å for the heavy atom overlays of residues 1–11 for 20 structures. Fig. 8 shows the backbone (*circles*) and heavy atom (*squares*) RMSDs per residue for the overlay of 20 structures. The error bars in Fig. 8 denote the range of deviations from the mean structure for each residue of a 10-structure ensemble. Residue Gln^6 is the least precisely defined residue for both side-chain and backbone atoms. The use of distance constraints from 1.8 to 6 Å for all the observed NOEs in the NMR data preferentially selects structures that comply with the longer distance constraints and deemphasizes the importance of shorter *i* to *i* + 1 constraints. This method selects the folded conforma-

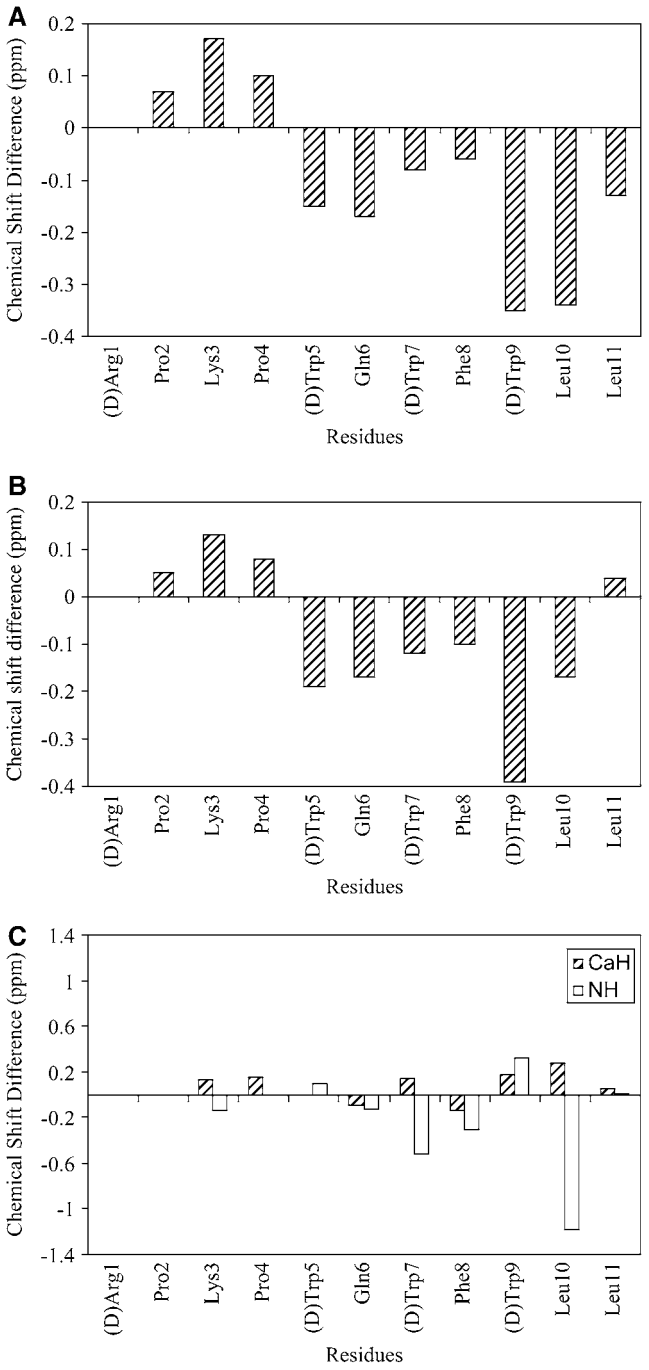

FIGURE 4 Chemical shift difference plots for SPA protons in water alone or in the presence of SDS micelles. The CαH chemical shift differences of SPA protons in water alone (*a*) or in the presence of SDS micelles (*b*) minus the random coil chemical shifts of Wishart et al. (51), respectively, are shown. A plot of the chemical shift differences of the identical NH and CαH protons from SPA in the presence of SDS micelles minus the chemical shifts of SPA in aqueous solution (*c*) is also shown. Shift differences >±0.2 ppm indicate a significant change in the chemical environment of the proton when going from aqueous to lipid milieus.

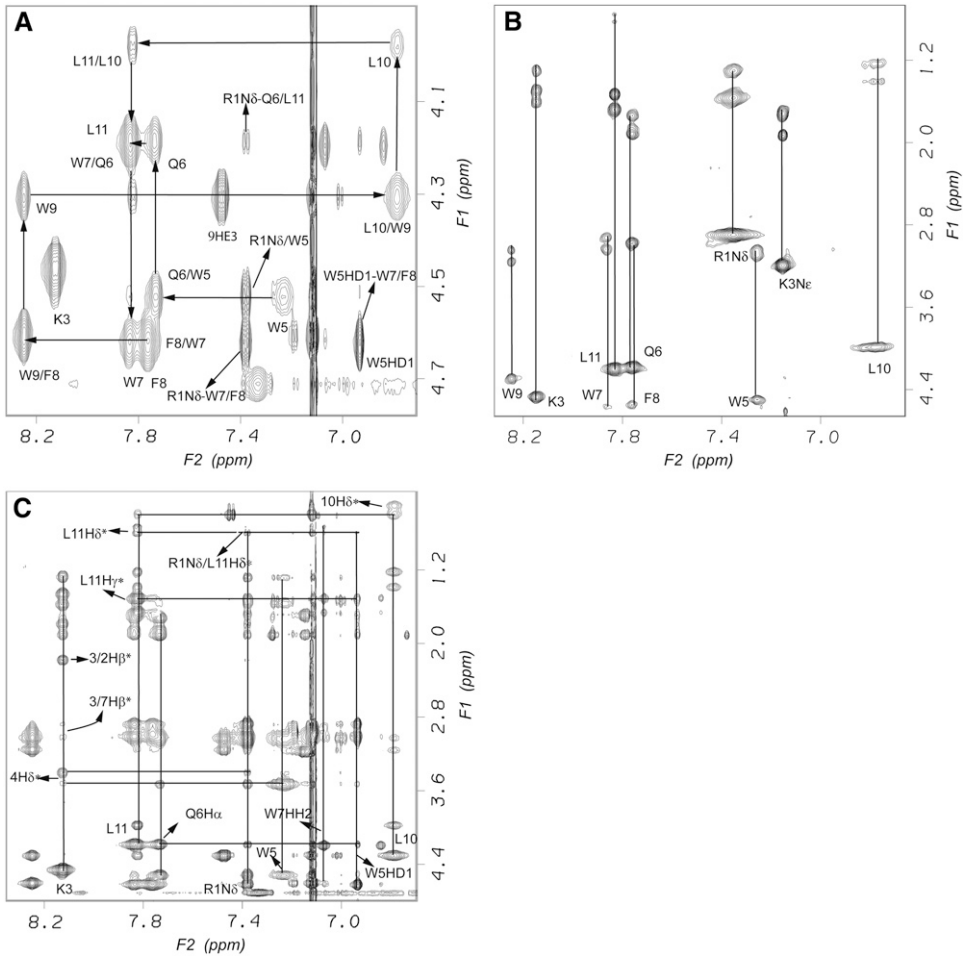

FIGURE 5 Selected regions of 500-MHz two-dimensional (2D) ^{1}H-NMR spectra of SPA in the presence of SDS micelles, including: (*a*) the NH proton to CαH proton correlation region of a 200-ms 2D NOESY spectrum, (*b*) the NH proton to CαH, CβH, CγH, and CδH proton correlation region of a 50-ms 2D TOCSY spectrum, (*c*) the NH proton to CαH, CβH, CγH, and CδH proton correlation region of a 200-ms 2D NOESY spectrum. Selected crosspeaks are labeled. All spectra were acquired on a solution of 1 mM SPA at pH 5.0 with 50 mM SDS and 25°C in 90% H_2O/10% D_2O.

tions defined by the majority of the NOE derived distance constraints and puts less emphasis in the structure calculations on the larger NOE volumes observed in the spectra.

After the structure calculations were completed we applied the programs PROCHECK_NMR and AQUA to the analysis of the NOE derived distance restraints and the structure of SPA (39). For the 83 constraints, 18 intraresidue distance restraints were found to be unnecessary by the AQUA criteria. The remaining 65 intraresidue distance restraints and the sequential, medium, and long-range interresidue constraints were all found to be nonredundant by the AQUA analysis. Two restraints were excluded by AQUA because they arose from the side chain amino protons of Lys^3 which normally are not visible in the spectra due to solvent exchange. In the presence of SDS micelles the exchange rate is slowed sufficiently that they are observable in the NOESY spectra and we observe crosspeaks to Pro^2 and Pro^4 side-chain protons to these protons.

The AQUA completeness score for SPA is 13% with the best defined portion of the peptide found in the C-terminal residues Trp^{9*} and Leu^{10} (completeness 20–25%). For the N-terminal portion of the peptide residues Lys^3, Pro^4, and Trp^{5*} have completeness scores of 10–15%. The Ramachandran analysis shows that all of the L-form amino acids in averaged SPA structure of 10 or 20 calculated structures are in allowed regions for their ϕ-ψ angles (not shown). As expected for D-form amino acids, the ϕ-ψ plots of the individually overlayed structures mostly show Trp^{5*}, Trp^{7*}, and Trp^{9*} in disallowed or generously allowed regions.

Finally, an examination of other 3D structure studies of similarly sized peptides reveals that the number of restraints we report here is very similar to literature values (e.g., (14, 15,18)). As short peptides are by their nature less proton dense than longer peptides or proteins fewer NOEs are observable. However, the presence of the long range NOE crosspeaks is unequivocal and our calculated structure represents a conformation that satisfies the complete set of 83 distance restraints without violation of a single distance bounds by the XPLOR criteria.

DISCUSSION

The interaction of a gastrointestinal peptide with lipid membranes may be important for its bioactivity in a number

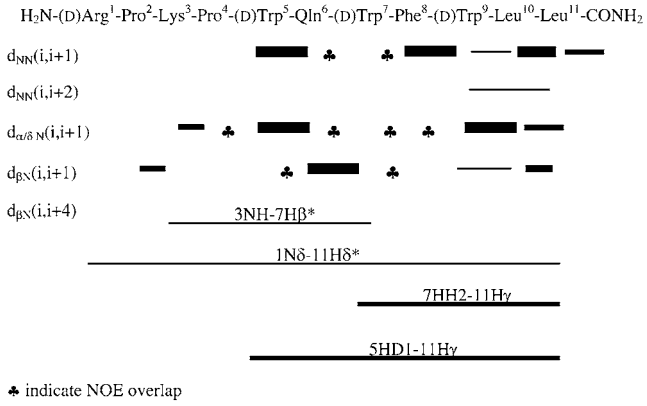

FIGURE 6 Selected NOE connectivity data used in the calculation of the tertiary structure of SPA in the presence of SDS micelles. The intensity of the bar classifies the NOE as a strong, medium, or weak signal. The clover symbol denotes connectivity that was not observed because of chemical shift degeneracy.

of steps from synthesis to action at a target receptor. In this work we examine the last step in this process where some have theorized that lipids in the membrane mediate the transport of peptides toward their receptors and the 3D conformation of the peptide that binds and activates the receptor (13). There is specific evidence that gastrin (40) and CCK (41,42) molecular forms interact with the CCK-B receptor via such a lipid-associated mechanism.

The work of Moroder and co-workers showed that gastrin and cholecystokinin fragments retained their ability to bind the CCK-B receptor with their N-termini anchored to the lipid bilayer by conjugation with lipid tails (40). Therefore, because lipo-derivatized gastrin and cholecystokinin bind to the CCK-B receptor with similar affinities and have primary sequence homology they may assume a common lipid-associated conformation that interacts with the same residues of the CCK-B receptor. In addition, as SPA is a competitive inhibitor of these peptides at the CCK-B receptor the lipid-associated conformation reported in this work could share a common spatial organization of peptide side chains that enables inhibition of CCK-B receptor binding by gastrin and cholecystokinin.

SPA in water

The CD, fluorescence, and NMR spectra for SPA in aqueous solution alone indicate a partially folded structure (Figs. 1–4). The CD spectra for SPA in water show a combination of random coil and turn-like features. The fluorescence spectra show that in water alone with equivalent concentrations of NATA and SPA, the NATA signal intensity is two-thirds that of SPA, which contains three tryptophan residues. Thus SPA in water alone must have a folded structure that affects the quantum yield of one or more the tryptophan residues. The NMR chemical shift data show residues with large changes from their random coil values for residues Trp^7*, Trp^9*, and Leu^{10}.

SPA in lipid

The CD, fluorescence, and NMR chemical shift data collected on SPA in the presence of SDS micelles show a major shift in tertiary structure compared to water alone. SPA binds to the lipid surface and alters the orientation of one or more of the three tryptophan side chains (Fig. 1) and alters the fluorescence of the indole rings (Fig. 2) compared to the structure in water alone. Of note the fluorescence spectrum of SPA in the presence of SDS micelles closely resembles that of NATA in the presence of SDS micelles instead of being one-third of the intensity. Based on comparisons to literature data we conclude that the tryptophan side chains are inserted into the water-lipid headgroup interfacial region of the SDS micelles (34–37).

The SPA chemical shift values in the presence of SDS micelles may be compared to Wishart random coil chemical shift values (Fig. 4; (38)). Selective chemical shift value changes are observed throughout the peptide in the presence of SDS micelles compared to their random coil chemical shift values. The largest changes are observed for Leu^{10} NH and Trp^5* backbone and side-chain NH values (-1.38, -1.00, and -0.76 ppm, respectively, δ_{SDS}-δ_{RC}). Other interesting large shifts from random coil values are observed for Pro^4 β and γ protons, the Trp^7* side-chain NH proton, and the backbone amide protons of Gln^6, Trp^7*, and Phe^8. The differences between both random coil and water only chemical shift values supports the conclusion that SPA has at least a partially folded structure in water alone and that this fold is altered with micelles association.

NMR structure determination

The BSNA SPA in the presence of SDS micelles folds into a unique tertiary structure that brings the N- and C-terminal

TABLE 2 Table of *i,i* + 2 and longer NOEs used in the structure calculations

i, i + 2	*i, i* + 3	*i, i* + 4	≥ *i, i* + 5
P4 Hδ Q6 HN	R1 HE P4 Hδ	K3 HN W7 Hβ*	R1 HE Q6 Hα
W5 Hα W7 HN	Q6 HN W9 Hβ*	W7 HH2 L11 Hβ*	W5 HD1 L11 Hδ*
W5 Hα W7 HE1		W7 HH2 L11 Hδ*	P4 Hδ* W9 HH2
W9 HD1 L11 Hδ*		W7 HE1 K3 Hγ*	
W9 HD1 L11 Hγ*		R1 HE W5 Hα	
F8 HD* L11 HN		W7 HH2 L11 Hγ*	
W7 HD1 W9 HE1			

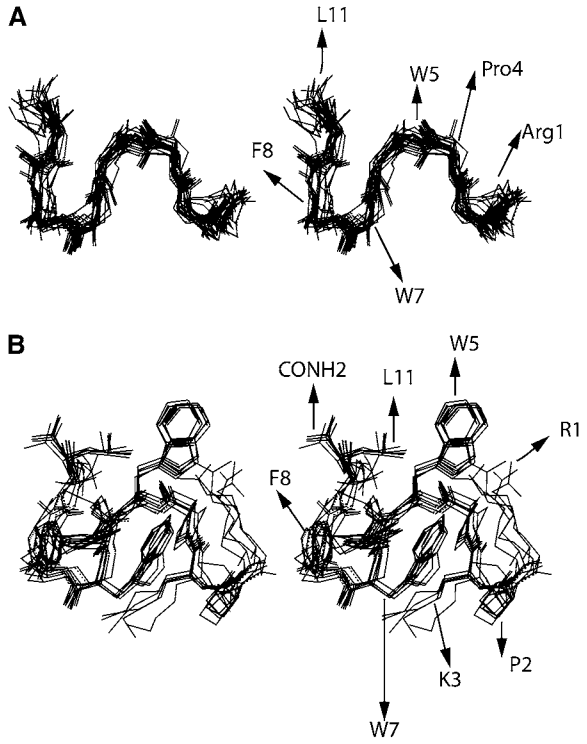

FIGURE 7 Stereo-views of the superposition of 20 coordinate sets of the backbone atoms (*a*) and six heavy atom coordinate sets (*b*) derived from 45 X-PLOR calculated structures derived from SPA proton NOE connectivity data observed in the presence of SDS micelles. Coordinate sets with no NOE violations >0.3 Å and the lowest NOE energies were selected for these overlays.

arginine and leucine residues near in space. This fold is stable enough for the observation of intermolecular NOEs and chemical shift perturbations. The long range NOEs in Table 2 and the other NOEs observed in 100- and 200-ms NOESY data were used to calculate the structure observed in Fig. 7.

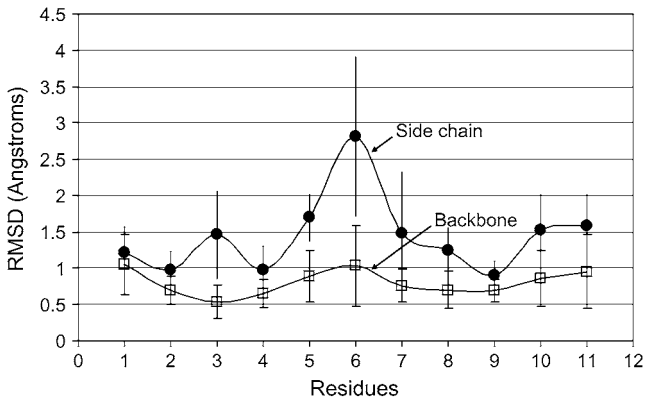

FIGURE 8 A plot of the RMSD per residue for the backbone (*open squares*) and heavy atom (*solid circles*) overlay of the 20 backbone or 20 heavy atom X-PLOR-calculated structures. The error bars denote the range of deviations from the mean structure for each residue of the 10 structure ensembles.

The compact structure can be loosely described as two nonstandard (Type IV) turns created by residues Arg[1]* through Pro[4], a connecting residue Trp[5]* and a second turn from Gln[6] to Trp[9]* (Fig. 7). These turns are called non standard because the mean angles derived over 20 structures do not fall into standard turn geometries, including; Type I (most common, −60, −30, and −90, 0 degree; ϕ-ψ angles for residues 2 and 3 of the turn) or Type III (helical, −60, −30, and −60, −30). The mean and standard deviation for the ϕ-ψ angles of 20 calculated structures for Pro[2] and Lys[3] are -76 ± 6, -59 ± 35, and -90 ± 32, 174 ± 13 degrees. The mean and standard deviation for the ϕ-ψ angles of 20 calculated structures for Trp[7]* and Phe[8] are -91 ± 72, -48 ± 66, and -144 ± 86, -56 ± 28.

The precision of the overlay indicates the tertiary structure of the backbone for residues Arg[1] to Leu[11] are well defined with the orientation of the side chains established best for Pro[2], Pro[4], Phe[8], and Trp[9]* (Fig. 8). The position of residue Qln[6], which is central to the structure of the peptide and the N-terminal residue Arg[1]* are less well defined by NOE distance constraints compared to neighboring residues. Therefore although the structural data presented is fully consistent with the CD, NMR, and fluorescence data we cannot exclude the presence of other conformers that result from conformational flexibility at the N-terminus and at Gln[6].

Ring current effects

The accuracy of the calculated structure is supported by the ring current shifts observed for the side-chain protons in the vicinity of the Trp[5]*, Trp[7]*, Phe[8], and Trp[9]* residues. Ring currents arise from the diamagnetic anisotropy of the aromatic rings and are often the major contributing factor to the observed conformation-dependent chemical shifts of side-chain protons (43). In general those protons oriented perpendicular to the face of the aromatic ring or in the plane of the ring will be shifted significantly upfield (≤ -0.2 ppm) or downfield ($\geq +0.2$ ppm), respectively, compared to their random coil chemical shift values when they are within four to five angstroms of the aromatic ring.

The chemical shift values of SPA in the presence of SDS micelles can be compared to the water only (WO) SPA chemical shift values determined in this work to assess changes that occur with micelle association. Based on the calculated structure residue Trp[5]* ring currents cause significant upfield shifts of protons on Arg[1]* (β, γ, and δ proton chemical shift values from −0.32 to −0.38 ppm, relative to the WO chemical shift values in Table 1, δ_{SDS}-δ_{WO}). Trp[5]* along with Trp[7]* influence the resonance position of Pro[4] (WO β and γ shifts from −0.24 to −0.65 ppm) protons. Trp[7]* ring currents shift downfield the side-chain protons of Lys[3] (WO δ and ε shifts from +0.30 to +0.51 ppm). Ring current effects are particularly noticeable for the Leu[10] backbone NH proton that shifts +1.19 ppm from the solution state value (attributed to the proximity of Phe[8] and Trp[9]*).

In addition, Leu^{10} side-chain CγH and CδH protons are shifted downfield by +0.72 and +0.37 ppm, respectively, from their water alone values. Residues Gln^6 and Leu^{11} chemical shift values are largely free of changes with micelle association.

The chemical shift differences between the peptide in water alone and in the presence of SDS micelles show large changes for Trp^{7}*, Phe^8, Trp^{9}*, and Leu^{10} (Fig. 4 *c*). These data suggest that the partially folded structure in aqueous solution binds the SDS micelles with an insertion of Trp^{7}*, Phe^8, Trp^{9}*, and Leu^{10} residues into the water-micelle interface.

SPA has different water-only and lipid-associated structures than substance P. For SPA, the differences in the CαH proton shifts from their random coil values indicates that residues Trp^{9}*, and Leu^{10} of SPA have a nonrandom coil-like structure in water only (Fig. 4 *a*). This view is supported by the CD data (Fig. 1). By contrast, substance P (Arg-Pro-Lys-Pro-Gln-Gln-Phe-Phe-Gly-Leu-Met-NH_2) water only NMR and CD data indicated a random coil solution structure (15). A direct comparison of structure perturbation upon lipid binding is the chemical shift differences of the identical peptide backbone amide and CαH protons between the solution and lipid associated states (Fig. 4 *c*). For SPA, these data show significant shifts in Trp^{7}*, Phe^8, Trp^{9}*, and Leu^{10} residues and smaller perturbations of the amino terminal Arg^{1}*, Pro^2, Lys^3, Pro^4, Trp^{5}*, Gln^6 residues upon lipid binding. By contrast, substance P shows significant shifts at Lys^3 and Gln^5-Met^{11} (15). A common element between substance P and SPA structures is the presence of C-terminal nonstandard turn structures while where they differ is in the N-terminal and mid-region structure.

Whitehead et al. found that D-amino acid substituted antagonists of the NK-1 receptor [D-Pro^2, D-Phe^7, D-Trp^9]-SP and [D-Arg^1, D-Pro^2, D-Trp^7, D-His^9]-SP had poorly defined helical mid-regions followed by a nonstandard β-turn structure at their C-termini (18). By contrast the tertiary structures of the NK receptor agonists—substance P, NKA and NKB—determined by Whitehead et al. in the presence of SDS micelles under identical conditions had helical regions that extended to residue 9 or 10. These authors conclude that the C-terminal nonstandard β-turn (containing residues 7, 8, and 9) enables antagonism at the NK-1 receptor. Therefore, in this context, the structure of the BNSA SPA ([D-Arg^1, D-$Trp^{5,7,9}$, Leu^{11}] substance P) determined in this work that contains a turn structure including residues 7, 8, and 9, is consistent with the model of Whitehead et al. in spite of the sequence differences between these peptides. By contrast the helical mid-regions of [D-Pro^2, D-Phe^7, D-Trp^9]-SP and [D-Arg^1, D-Pro^2, D-Trp^7, D-His^9]-SP are replaced by a nonstandard turn in the N-terminus of SPA. We propose that the substitution of D-amino acids and the presence of Trp^{5}* in particular leads to the unique series of two nonstandard turns that enable this peptide to act as an antagonists at not only the NK_1 receptor but also the bradykinin, vasopressin, GRP, bombesin, and gastrin receptors (7).

Based on the NMR chemical shift values observed in this work and comparisons to the previously determined detailed model of substance P/SDS micelle association we propose that C-terminus of SPA inserts into the water-lipid interface via residues Trp^{7}*, Phe^8, Trp^{9}*, and Leu^{10}. Where SPA differs from substance P and the other substance P analogs is in the N-terminal turn structure. In the presence of SDS micelles a well-defined nonstandard turn is formed consisting of Arg^{1}*, Pro^2, Lys^3, and Pro^4. We propose that the charged side chains of Arg^{1}* and/or Lys^3 form salt bridges with sulfate headgroups and the hydrophobic segments of these residues and those of the neighboring proline amino acids act to stabilize a well-defined turn structure in SPA. Evidence for the interaction of Lys^3 amino group with sulfate headgroups is the observation of the side chain εNH_3 signal in the spectra collected in the presence of SDS micelles but not in the water alone spectra.

SPA ([D-Arg^1, D-$Trp^{5,7,9}$, Leu^{11}] substance P) inhibits the activity of a number of G-protein coupled neuropeptide receptors, including: bradykinin, vasopressin, gastrin-releasing peptide (GRP), bombesin, and gastrin receptors (44–46). By contrast, spantide ([D-Arg^1, D-$Trp^{7,9}$, Leu^{11}] substance P) has been shown to be a NK_1, NK_2, and bombesin receptor antagonists but does not inhibit the activity of cholecystokinin, gastrin, or secretin peptides (47–49). Spantide only differs from SPA by the substitution of a D-Trp for Gln at position 5.

The position 5 substitution alters the tertiary structure of SPA compared to spantide in water alone and in the presence of SDS micelles. Bello et al. showed CD spectra for spantide in 0.1 M phosphate buffer at pH 7 that show [−]200 and [−]225 nm bands (50). In our pH 5 water alone spectra we observed [−]200, [−]213, and [+]229 nm bands. For spantide in 40 mM SDS and pH 6.8, Di Bello et al. observe [+]190, [−]200, and [−]226 nm bands with the ratio of the [−]200 to [−]226 band intensities being 0.8. In this work at pH 5.0 and 50 mM SDS no [+]190 nm band was observed and the relative ratios of the [−]200:[−]226 nm intensities was 0.4.

The fluorescence spectrum of spantide in aqueous solution does not change significantly upon addition of SDS micelles and displays emission maxima of ~337 nms and similar broad peak shape for both solution conditions. By contrast, for SPA there is a 42% decrease in the observed intensity with the addition of SDS micelles with minimal shift in the observed maxima. We conclude that the structures of SPA and spantide in SDS micelles are different because of the substitution of a D-Trp for Gln at position 5 and that these unique conformations play a role in the altered receptor pharmacology observed for these two substance P analogs.

CONCLUSIONS

Because SPA is a competitive inhibitor of mitogenic peptide hormones such as bombesin, cholecystokinin, and gastrin,

the receptor bound conformation of SPA and these ligands could have a region of tertiary structure identity that interacts at a similar receptor binding site. Thus the 3D conformation of SPA in the presence of lipids may represent the spatial arrangement of functional groups found in the receptor bound state of the peptide. If so this conformation would be useful in the design of nonpeptide antagonists and agonists for the treatment of pancreatic, colon, and prostate cancers. The use of lipid associated structures of peptide ligands for design of analogs active at G-protein coupled receptors is limited in that receptor-ligand interactions are not directly interrogated. The value of the structures determined to date will become apparent when sufficient receptor and appropriate methods to reconstitute them in their biologically active receptor associated form become available for detailed NMR studies (e.g., (10)).

This work was supported in part by the National Cancer Institute, UCLA SPORE in Lung Cancer 1 P50 CA90388- Section III, the CURE Digestive Diseases Research Center grant DK 41301, National Institutes of Health grant DK56805, and the Medical Research Service of the Veterans Health Service.

REFERENCES

1. Ji, T. H., M. Grossmann, and I. Ji. 1998. G protein-coupled receptors. I. Diversity of receptor-ligand interactions. *J. Biol. Chem.* 273:17299–17302.
2. Rozengurt, E. 2002. Neuropeptides as growth factors for normal and cancerous cells. *Trends Endocrinol. Metab.* 13:128–134.
3. Heasley, L. E. 2001. Autocrine and paracrine signaling through neuropeptide receptors in human cancer. *Oncogene.* 20:1563–1569.
4. Seckl, M. J., T. Higgins, F. Widmer, and E. Rozengurt. 1997. [D-Arg^{1}, D-Trp^{5,7,9},Leu^{11}]substance P: a novel potent inhibitor of signal transduction and growth in vitro and in vivo in small cell lung cancer cells. *Cancer Res.* 57:51–54.
5. MacKinnon, A. C., C. Waters, I. Rahman, N. Harani, R. Rintoul, C. Haslett, and T. Sethi. 2000. [Arg^{6}, D-Trp^{7,9}, N$_{me}$Phe^{8}]-substance P(6–11) (antagonist G) induces AP-1 transcription and sensitizes cells to chemotherapy. *Br. J. Cancer.* 83:941–948.
6. Langdon, S., T. Sethi, A. Ritchie, M. Muir, J. Smyth, and E. Rozengurt. 1992. Broad spectrum neuropeptide antagonists inhibit the growth of small cell lung cancer in vivo. *Cancer Res.* 52:4554–4557.
7. Seckl, M. J., T. Higgins, and E. Rozengurt. 1996. [D-Arg^{1}, D-Trp^{5,7,9}, Leu^{11}]substance P coordinately and reversibly inhibits bombesin- and vasopressin-induced signal transduction pathways in Swiss 3T3 cells. *J. Biol. Chem.* 271:29453–29460.
8. Guha, S., G. Eibl, K. Kisfalvi, R. S. Fan, M. Burdick, H. Reber, O. J. Hines, R. Strieter, and E. Rozengurt. 2005. Broad-spectrum G protein-coupled receptor antagonist, [D-Arg^{1}, D-Trp^{5,7,9}, Leu^{11}]SP: a dual inhibitor of growth and angiogenesis in pancreatic cancer. *Cancer Res.* 65:2738–2745.
9. Prabhu, A., A. Malde, E. Coutinho, and S. Srivastava. 2005. Solution conformation of substance P antagonists-[D-Arg^{1}, D-Trp^{7,9}, Leu^{11}]-SP, [D-Arg^{1}, D-Pro^{2}, D-Trp^{7,9}, Leu^{11}]-SP and [D-Pro^{2}, D-Trp^{7,9}]-SP by CD, NMR and MD simulations. *Peptides.* 26: 875–885.
10. Inooka, H., T. Ohtaki, O. Kitahara, T. Ikegami, S. Endo, C. Kitada, K. Ogi, H. Onda, M. Fujino, and M. Shirakawa. 2001. Conformation of a peptide ligand bound to its G-protein coupled receptor. *Nat. Struct. Biol.* 8:161–165.
11. McDonnell, P. A., and S. J. Opella. 1993. Effect of detergent concentration on multidimensional solution NMR spectra of membrane proteins in micelles. *J. Magn. Res. Series B.* 102:120–125.
12. Kallick, D. H., M. R. Tessmer, C. R. Watts, and C. Y. Li. 1995. The use of dodecylphosphocholine micelles in solution NMR. *J. Magn. Res. B.* 109:60–65.
13. Schwyzer, R. 1995. 100 years lock-and-key concept: are peptides shaped and guided to their receptors by the target cell membrane. *Biopolymers.* 37:5–16.
14. Auge, S., B. Bersch, M. Tropis, and A. Milon. 2000. Characterization of substance P-membrane interaction by transferred nuclear Overhauser effect. *Biopolymers.* 54:297–306.
15. Keire, D. A., and T. G. Fletcher. 1996. The conformation of substance P in lipid environments. *Biophys. J.* 70:1716–1727.
16. Keire, D. A., and M. Kobayashi. 1998. The orientation and dynamics of substance P in lipid environments. *Protein Sci.* 7:2438–2450.
17. Wymore, T., and T. C. Wong. 1999. Molecular dynamics study of substance P peptides partitioned in a sodium dodecylsulfate micelle. *Biophys. J.* 76:1213–1227.
18. Whitehead, T. L., S. D. McNair, C. E. Hadden, J. K. Young, and R. P. Hicks. 1998. Membrane-induced secondary structures of neuropeptides: a comparison of the solution conformations adopted by agonists and antagonists of the mammalian tachykinin NK1 receptor. *J. Med. Chem.* 41:1497–1506.
19. Hong, S. Y., J. E. Oh, and K. H. Lee. 1999. Effect of D-amino acid substitution on the stability, the secondary structure, and the activity of membrane-active peptide. *Biochem. Pharmacol.* 58:1775–1780.
20. Rothemund, S., M. Beyermann, E. Krause, G. Krause, M. Bienert, R. S. Hodges, B. D. Sykes, and F. D. Sonnichsen. 1995. Structure effects of double D-amino acid replacements: a nuclear magnetic resonance and circular dichroism study using amphipathic model helices. *Biochemistry.* 34:12954–12962.
21. Braunschweiler, L., and R. R. Ernst. 1983. Coherence transfer by isotropic mixing: application to proton correlation spectroscopy. *J. Magn. Res.* 53:521–528.
22. Jeener, J., B. H. Meier, P. Bachmann, and R. R. Ernst. 1979. Investigation of exchange processes by two-dimensional NMR spectroscopy. *J. Magn. Res.* 71:4546–4554.
23. Sklenar, V. 1995. Suppression of radiation damping in multidimensional NMR experiments using magnetic field gradients. *J. Magn. Res.* A114:132–135.
24. Marion, D., and K. Wuthrich. 1983. Application of phase sensitive two-dimensional correlated spectroscopy (COSY) for measurements of ^{1}H-^{1}H spin-spin coupling constants in proteins. *Biochem. Biophys. Res. Commun.* 113:967–974.
25. States, D. J., R. A. Haberkorn, and D. J. Ruben. 1982. A two-dimensional nuclear Overhauser experiment with pure absorption phase in four quadrants. *J. Magn. Res.* 48:286–292.
26. Piotto, M., V. Saudek, and V. Sklenar. 1992. Gradient-tailored excitation for single-quantum NMR spectroscopy of aqueous solutions. *J. Biomol. NMR.* 2:661–665.
27. Hwang, T., and A. Shaka. 1995. Water suppression that works. excitation sculpting using arbitrary wave-forms and pulsed-field gradients. *J. Magn. Res. Series A.* 112:275–279.
28. Brunger, A. T. 1992. X-PLOR: Version 3.1. A System for X-ray Crystallography and NMR. Yale Unviersity Press. New Haven, Conn.
29. Wuthrich, K., M. Billeter, and W. Braun. 1983. Pseudo-structures for the 20 common amino acids for use in studies of protein conformations by measurement of intramolecular proton-proton distance constraints with nuclear magnetic resonance. *J. Mol. Biol.* 169:949–961.
30. Perczel, A., and M. Hollosi. 1996. Turns. *In* Circular Dichroism and the Conformational Analysis of Biomolecules. G. Fasman, editor. Plenum Press, New York. 285–380.
31. Woody, R. W. 1994. Contributions of tryptophan side chains to the far-ultraviolet circular dichroism of proteins. *Eur. Biophys. J.* 23:253–262.

32. Ladokhin, A. S., M. E. Selsted, and S. H. White. 1999. CD spectra of indolicidin antimicrobial peptides suggest turns, not polyproline helix. *Biochemistry*. 38:12313–12319.
33. Ladokhin, A. S., S. Jayasinghe, and S. H. White. 2000. How to measure and analyze tryptophan fluorescence in membranes properly, and why bother? *Anal. Biochem*. 285:235–245.
34. Snel, M. M., R. Kaptein, and B. de Kruijff. 1991. Interaction of apocytochrome c and derived polypeptide fragments with sodium dodecyl sulfate micelles monitored by photochemically induced dynamic nuclear polarization ^{1}H NMR and fluorescence spectroscopy. *Biochemistry*. 30:3387–3395.
35. de Kroon, A. I., M. W. Soekarjo, J. de Gier, and B. de Kruijff. 1990. The role of charge and hydrophobicity in peptide-lipid interaction: a comparative study based on tryptophan fluorescence measurements combined with the use of aqueous and hydrophobic quenchers. *Biochemistry*. 29:8229–8240.
36. Jacobs, R. E., and S. H. White. 1989. The nature of the hydrophobic binding of small peptides at the bilayer interface: implications for the insertion of transbilayer helicies. *Biochemistry*. 28:3421–3437.
37. de Planque, M. R., B. B. Bonev, J. A. Demmers, D. V. Greathouse, R. E. Koeppe 2nd, F. Separovic, A. Watts, and J. A. Killian. 2003. Interfacial anchor properties of tryptophan residues in transmembrane peptides can dominate over hydrophobic matching effects in peptide-lipid interactions. *Biochemistry*. 42:5341–5348.
38. Wishart, D. S., C. G. Bigam, A. Holm, R. S. Hodges, and B. D. Sykes. 1995. ^{1}H, ^{13}C and ^{15}N random coil NMR chemical shifts of the common amino acids. I. Investigations of nearest-neighbor effects. *J. Biomol. NMR*. 5:67–81.
39. Laskowski, R. A., J. A. Rullmannn, M. W. MacArthur, R. Kaptein, and J. M. Thornton. 1996. AQUA and PROCHECK-NMR: programs for checking the quality of protein structures solved by NMR. *J. Biomol. NMR*. 8:477–486.
40. Moroder, L. 1997. On the mechanism of hormone recognition and binding by the CCK-B/gastrin receptor. *J. Pept. Sci*. 3:1–14.
41. Moroder, L., R. Romano, W. Guba, D. F. Mierke, H. Kessler, C. Delporte, J. Winand, and J. Christophe. 1993. New evidence for a membrane-bound pathway in hormone receptor binding. *Biochemistry*. 32:13551–13559.
42. Giragossian, C., and D. F. Mierke. 2002. Intermolecular interactions between cholecystokinin-8 and the third extracellular loop of the cholecystokinin-2 receptor. *Biochemistry*. 41:4560–4566.
43. Perkins, S. J., and K. Wuthrich. 1979. Ring current effects in the conformation dependent NMR chemical shifts of aliphatic protons in the basic pancreatic trypsin inhibitor. *Biochim. Biophys. Acta*. 576:409–423.
44. MacKinnon, A. C., R. A. Armstrong, C. M. Waters, J. Cummings, J. F. Smyth, C. Haslett, and T. Sethi. 1999. [Arg^{6},D-Trp^{7,9},N$_{me}$Phe^{8}]-substance P (6–11) activates JNK and induces apoptosis in small cell lung cancer cells via an oxidant-dependent mechanism. *Br. J. Cancer*. 80:1026–1034.
45. Seckl, M. J., R. H. Newman, P. S. Freemont, and E. Rozengurt. 1995. Substance P-related antagonists inhibit vasopressin and bombesin but not 5′-3-O-(thio)triphosphate-stimulated inositol phosphate production in Swiss 3T3 cells. *J. Cell. Physiol*. 163:87–95.
46. Sinnett-Smith, J., C. Santiskulvong, J. Duque, and E. Rozengurt. 2000. [D-Arg^{1}, D-Trp^{5,7,9}, Leu^{11}]Substance P inhibits bombesin-induced mitogenic signal transduction mediated by both G_q and G_{12} in Swiss 3T3 cells. *J. Biol. Chem*. 275:30644–30652.
47. Janecka, A., J. Poels, J. Fichna, K. Studzian, and J. Vanden Broeck. 2005. Comparison of antagonist activity of spantide family at human neurokinin receptors measured by aequorin luminescence-based functional calcium assay. *Regul. Pept*. 131:23–28.
48. Jensen, R. T., D. H. Coy, Z. A. Saeed, P. Heinz-Erian, S. Mantey, and J. D. Gardner. 1988. Interaction of bombesin and related peptides with receptors on pancreatic acinar cells. *Ann. N. Y. Acad. Sci*. 547: 138–149.
49. Yachnis, A. T., J. N. Crawley, R. T. Jensen, M. M. McGrane, and T. W. Moody. 1984. The antagonism of bombesin in the CNS by substance P analogues. *Life Sci*. 35:1963–1969.
50. Di Bello, C., A. Scatturin, G. D'Auria, M. Gargiulo, L. Paolillo, E. Trivellone, and R. De Castiglione. 1991. Fluorescence, CD, and NMR studies on spantide, a bombesin and substance P antagonist. *Biopolymers*. 31:643–652.
51. Wishart, D. S., B. D. Sykes, and F. M. Richards. 1992. The chemical shift index: a fast and simple method for the assignment of protein secondary structure through NMR spectroscopy. *Biochemistry*. 31: 1647–1651.